Accepted Manuscript

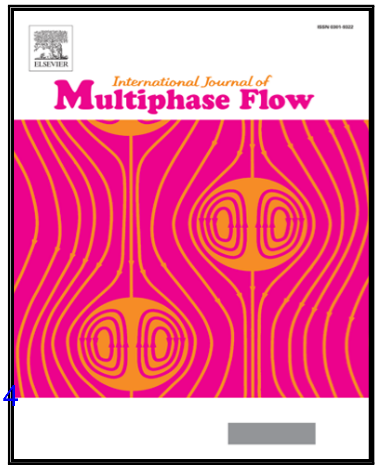

Inhomogeneity and anisotropy in Eulerian-Eulerian near-wall modelling

M. Riella, R. Kahraman, G.R. Tabor

PII: S0301-9322(18)30493-2
DOI: https://doi.org/10.1016/j.ijmultiphaseflow.2019.01.014
Reference: IJMF 2963

To appear in: *International Journal of Multiphase Flow*

Received date: 10 July 2018
Revised date: 16 December 2018
Accepted date: 31 January 2019

Please cite this article as: M. Riella, R. Kahraman, G.R. Tabor, Inhomogeneity and anisotropy in Eulerian-Eulerian near-wall modelling, *International Journal of Multiphase Flow* (2019), doi: https://doi.org/10.1016/j.ijmultiphaseflow.2019.01.014

Highlights

- A pressure-velcity model to account for the no permeability constraint is proposed for E-E simulations.
- The model is derived within a Reynolds-Averaged Two-Fluid model framework and implemented within the open-source CFD toolbox OpenFOAM.
- The approach is capable of accounting for the strong near-wall inhomogeneity, a flow feature that hitherto has been neglected in Eulerian-Eulerian modelling.
- The predictions reveal that the approach proposed herein can lead to a satisfactory agreement across all turbulence statistics paving the way for the correct prediction of more complex mechanisms.
- The source code of the recently developed solver ratfmFoam and supplementary material used in this work is made available online.

Inhomogeneity and anisotropy in Eulerian-Eulerian near-wall modelling

M. Riella[a,*], R. Kahraman[b], G. R. Tabor[a]

[a] *College of Engineering, Mathematics and Physical Sciences, University of Exeter, North Park Road, Exeter EX4 4QF, UK*
[b] *HiETA Technologies Ltd, Bristol & Bath Science Park, Dirac Crescent, Emersons Green, Bristol, BS16 7FR, UK*

Abstract

This paper tackles the issue of image vorticity in turbulent Eulerian-Eulerian simulations. A pressure-velocity model to account for the no permeability constraint on the fluid- and particle-phase wall normal stress components is proposed. The pressure-velocity model is derived with in a Reynolds-Averaged Two-Fluid model (RA-TFM) framework and is implemented within the open-source CFD toolbox OpenFOAM. We demonstrate that this approach is capable of accounting for the strong near-wall inhomogeneity, a flow feature that hitherto has been neglected in Eulerian-Eulerian modelling. Simulation predictions are validated against benchmark Direct Numerical Simulation data and show a promising step forward in near-wall modelling in Eulerian-Eulerian simulations. The predictions reveal that the approach proposed herein can lead to a satisfactory agreement across all turbulence statistics paving the way for the correct prediction of more complex mechanisms. Finally, the source code of the recently developed solver `ratfmFoam` and supplementary material used in this work is made available online.

Keywords: `RA-TFM`, `Near-wall`, `Eulerian-Eulerian`, `v2f`, `turbulence`

*Corresponding author
Email address: `mjr214@exeter.ac.uk` (M. Riella)

1. Introduction

The near-wall behaviour of particle-laden fluid behaviour has been a challenging topic for researchers over the preceding decades. Modelling the highly inhomogeneous near-wall region in a turbulent shear flow has proved difficult even in single phase flows [1]. One phenomenon in particular that has proven challenging is the so-called image vorticity [2, 3] that is caused by the kinematic blocking by the wall. This non-local effect on the Reynolds stress arises due to the physical inviscid boundary condition i.e. the no-flux condition on the normal component of velocity $\mathbf{u} \cdot \mathbf{n} = 0$. This effect results in a highly anisotropic distribution amongst the Reynolds stress components in the vicinity of a wall, mainly it is felt as a suppression of energy transfer into the wall-normal component.

To circumvent these issues Durbin [4] proposed a pressure-velocity model based on the Reynolds-Stress wall-normal component and an elliptical relaxation function to account for the kinematic blocking effect. In single-phase simulations this approach has proven fruitful [5, 6, 4, 7, 8, 9], with results showing distinct improvements over simulations with damping-functions and in particular wall-functions, as neither can account for the so-called stagnation-point anomaly or imposed pressure gradients.

Owing largely to its maturity and complexity, research in turbulent near-wall fluid-particle modelling in an Eulerian-Eulerian (E-E) framework has been sparse. One notably study is that of Rizk and Elghobashi [10] in which a theoretical study was carried out to ascertain the effects of increasing volume fraction on the mean velocity profile. They found that the log-layer broke down in their model speculating that a standard wall-function may not be representative of particle-laden flow. This postulation was somewhat corroborated by Vreman et al. [11] who showed that the log-layer was retained but resulted in an adjustment of the von Karman "constant". In addition to this, Benyahia et al. [12] showed that the effect of the particle phase could be included in the wall-function in an ad-hoc manner which allows the particle phase to influence the fluid phase velocity when the particle-fluid co-variance remained correlated.

The use of single-phase wall functions in E-E simulations are abundant in literature [13, 14, 15, 16, 17]. The wall functions are applied to the fluid phase regardless of the volume fraction in which complicated one- or two-way coupling effects can play a role. Moreover, the universal form of the log-layer neglects pressure gradients, with the addition of particles an induced hydro-static pressure gradient can commonly be found in the boundary layer. Attempts to circumvent this issue through damping functions have been used [18, 19, 10, 20]. This introduces further complications with arbitrarily matching experimental/Direct Numerical Simulation (DNS) in new or more complicated geometries. The drawbacks of damping-functions are well known i.e. their arbitrariness and dampening the incorrect scale [21].

In the literature E-E simulations in the near-wall region rarely predict the correct turbulence statistics in the particle phase. Moreover, the particle-phase wall normal component can not be correctly predicted due to the $k - \varepsilon$ modelling assumptions i.e. the eddy-viscosity approximation for the pressure-velocity redistribution terms. In the particle phase this is particularly problematic as the wall-normal component is known to govern segregation towards the wall [22, 23] and can inhibit the correct volume fraction distribution.

A more fundamental explanation can be given when considering E-E (Two-Fluid Models) models. In the current E-E the correlated fluctuating component of the particle phase is equated to the uncorrelated fluctuating energy of the particle phase. This error was first elucidated by Fevrier et al. [24] in which the partitioning effect of particle inertia was shown to give rise to two different contributions to the particle phase energy, namely correlated and uncorrelated energy. This distinction is crucial in both collisional and non-collisional flow Fox [25], Fevrier et al. [24] and has been shown to predict the correct physics in comparison with the current E-E models in which the distinction is not made Riella et al. [26].

In the near-wall region this distinction can prove particularly crucial. As the Stokes number, St increases as the wall is approached the correlated particle-phase energy k_p is dissipated into uncorrelated particle-phase energy Θ_p. This stokes dependent behaviour is vital to predicting the correct distribution of particle-phase energy in the near-wall region. Without accounting for this behaviour, in combination with wall-functions or damping functions it is clear why the near-wall region has proven particularly challenging and has received little attention Peirano and Leckner [27].

Within the context of near-wall modelling the turbulence constants may need to be changed to account for the presence of the particles. Bolio et al. [18] reported no significant changes in C_1, C_2, σ_k and σ_ε. Despite this Fox [25] has shown that there in-fact is a small dependence on the Stokes number for homogeneous-shear flow - change in C_2. In the near-wall region the picture is complicated further and no experimental or DNS data exists. In this study we do not consider the influence of the turbulence constants but it is recognised here that with increased mass loading and stokes number the constants may need to be changed. Within the near-wall region this is particularly uncertain and more research needs to be done.

In this paper we propose a pressure-velocity model in both phases. Within the E-E framework we assume continuous inter-penetrating phenomena and both phases share their pressure field. Recognising this is crucial for justifying the modelling decisions. We propose that the pressure reflection caused by the wall is felt in both phases and as a result we can derive a pressure-velocity model for each phase. The suppression of the wall-normal component enters the Reynolds stress transport equation through the velocity-pressure gradient correlation and is a term that appears in the Reynolds stress equation for both phases.

To investigate the applicability of the model we apply it to a benchmark channel flow case. The pressure-velocity model is derived and applied with a Reynolds-Averaged Two-Fluid Model framework [25, 26]. Predictions are compared against the Direct-Numerical-Simulation data of Marchioli and colleagues [28]. Two cases are simulated with increasing Stokes number to highlight the partitioning effect of particle inertia. Additionally, a mesh independence study is carried out, due to the necessary resolution of the mesh to resolve the boundary layer, to ascertain the sensitivity of the models predictions.

2. Numerical Model

The RA-TFM governing equations along with the recently derived multiphase $\overline{v_f^2} - f$ model [29] can be found in Table 1. The derivation of which can be found in Appendix A. Due to flow regime under consideration the buoyancy induced terms are neglected throughout this work. For a thorough description of the model the reader is referred to Fox [25]. The reader should note that the variables presented herein are the Phase-Averaged (PA) variables and their definitions can be found in Table 5.

The particle phase turbulent kinetic energy transport equation reads:

$$\begin{aligned}\frac{\partial(\alpha_p\rho_p k_p)}{\partial t} + \nabla\cdot(\alpha_p\rho_p k_p \mathbf{u}_p) = \nabla\cdot\Big(\mu_p + \frac{\mu_{pt}}{\sigma_{pk}}\Big)\nabla k_p + \alpha_p\rho_p\Pi_p - \alpha_p\rho_p\varepsilon_p \\ +2\beta(k_{fp} - k_p)\end{aligned} \tag{1}$$

The first term on the RHS is the particle phase turbulent kinetic dissipation energy flux. The second term Π_p is kinetic energy production due to mean shear with the third term being its dissipation. The remaining term is the coupling terms due to velocity correlations. The coupling terms take the form of $k_{fp} = \sqrt{k_f k_p}$ and $\varepsilon_{fp} = \sqrt{\varepsilon_f \varepsilon_p}$. These terms represent the fluid-velocity covariance. The particle phase turbulent kinetic energy dissipation transport equation reads:

$$\begin{aligned}\frac{\partial(\alpha_p\rho_p\varepsilon_p)}{\partial t} + \nabla\cdot(\alpha_p\rho_p\varepsilon_p\mathbf{u}_p) = \nabla\cdot\Big(\mu_p + \frac{\mu_{pt}}{\sigma_{pk}}\Big)\nabla\varepsilon_p + \frac{\varepsilon_p}{k_p}(C_{\varepsilon 1}\alpha_p\rho_p\Pi_p - C_{\varepsilon 2}\alpha_p\rho_p\varepsilon_p) \\ +2\beta(\varepsilon_{fp} - \varepsilon_p)\end{aligned} \tag{2}$$

The first term on the RHS is the particle phase turbulent kinetic dissipation energy flux. The second term Π_p is kinetic energy production due to mean shear with the third term being its dissipation. The remaining term is the coupling term due to velocity correlations. The granular temperature transport equation reads:

$$\begin{aligned}\frac{3}{2}\Big[\frac{\partial(\alpha_p\rho_p\Theta_p)}{\partial t} + \nabla\cdot(\alpha_p\rho_p\Theta_p\mathbf{u}_p)\Big] = \nabla\cdot\Big(\kappa_\Theta + \frac{3\mu_{pt}}{2Pr_{pt}}\Big)\nabla\Theta_p + 2\mu_p\overline{\mathbf{S}}_\mathbf{p} : \overline{\mathbf{S}}_\mathbf{p} \\ -p_p\nabla\cdot\mathbf{u}_p + \alpha_p\rho_p\varepsilon_p - 3\beta\Theta_p - \gamma\end{aligned} \tag{3}$$

The first term on the RHS is the PA granular temperature flux which is made up of two contributions, the granular temperature flux and the turbulent granular flux. The former is the granular conductivity of which there are various formulations in the literature. Here the formulation of Syamlal and O'Brien [30] is used as it correctly tends to zero in the dilute limit [31]. The latter term is the turbulent flux and includes the particle turbulent viscosity. The second term is a laminar source term due to viscous stresses. The third term is a pressure dilation term which accounts for compressibility. The fourth term is of particular interest as it represents the turbulent particle kinetic energy dissipation which appears here as a positive source term. The physical interpretation of this means that as large scale particle turbulent kinetic energy is dissipated, small scale granular temperature is produced. The two remaining terms represent decrease of granular temperature due to drag and decrease of granular temperature due to inelastic collisions.

2.1. Derivation of particle-phase pressure-velocity model

In order to derive the transport equation for the particle-phase wall normal component one needs to begin at the exact RA Reynolds stress transport equation. It can be found by Reynolds-Averaging the PA velocity tensor transport equation and subtracting the PA particle-phase mean velocity tensor transport equation. A rigorous derivation can be found in [32] and for the sake of brevity will not be presented here.

$$
\begin{aligned}
\frac{\partial \langle \alpha_p \rangle \langle \mathbf{u}''_p \otimes \mathbf{u}''_p \rangle_p}{\partial t} + \nabla \cdot \langle \alpha_p \rangle \langle \mathbf{u}_p \rangle_p \otimes \langle \mathbf{u}''_p \otimes \mathbf{u}''_p \rangle_p &= -\nabla \cdot \langle \alpha_p \rangle \langle \mathbf{u}''_p \otimes \mathbf{u}''_p \otimes \mathbf{u}''_p \rangle_p \\
&- \underbrace{\langle \alpha_p \rangle (\langle \mathbf{u}''_p \otimes \mathbf{u}''_p \rangle_p \cdot \nabla \langle \mathbf{u}_p \rangle_p)}_{\text{Production}} + \frac{1}{\rho_p} \nabla \cdot \langle \overline{\boldsymbol{\sigma}}_p \otimes \mathbf{u}''_p \rangle - \frac{1}{\rho_p} \nabla \langle p_p \mathbf{u}''_p \rangle \\
+ \underbrace{\frac{1}{\rho_p} \langle p_p \nabla \mathbf{u}''_p \rangle}_{\text{pressure strain, } \phi_{p,yy}} - \underbrace{\frac{1}{\rho_p} \langle \overline{\boldsymbol{\sigma}}_p \cdot \nabla \mathbf{u}''_p \rangle}_{\text{dissipation, } \varepsilon_{p,yy}} &+ \langle \alpha_p \rangle \beta (\underbrace{\langle \mathbf{u}'''_f \otimes \mathbf{u}''_p \rangle_p - \langle \mathbf{u}''_p \otimes \mathbf{u}''_p \rangle_p}_{\text{velocity correlations}})
\end{aligned}
\quad (4)
$$

We postulate that an imaginary particle phase wall normal component transport equation can be derived with adequate closure to the terms presented in Eq. 4. Firstly, we recognise that the production term is a function of the mean flow gradients in the stream-wise direction therefore it is dropped.

The velocity correlations which arise due to phase coupling are dominant in this work and have been shown to display the correct behaviour in one-way coupled flow Fox [25]. We therefore adopt the same form for their closure by setting the co-variance of the fluctuations $\langle \mathbf{u}'''_f \otimes \mathbf{u}''_p \rangle_p = \overline{v^2_{fp}} = \sqrt{\overline{v^2_p}\,\overline{v^2_f}}$.

Following the standard approach used in classic eddy-viscosity turbulence models, the divergence terms appearing in the transport equation are closed by the eddydiffusivity approximation [1].

$$\nabla \cdot \left[\frac{\mu_{pt}}{\sigma_{pk}} \nabla \langle \mathbf{u}_p'' \otimes \mathbf{u}_p'' \rangle_p \right] \approx -\nabla \cdot \langle \alpha_p \rangle \langle \mathbf{u}_p'' \otimes \mathbf{u}_p'' \otimes \mathbf{u}_p'' \rangle_p + \frac{1}{\rho_p} \nabla \cdot \langle \overline{\boldsymbol{\sigma}}_p \otimes \mathbf{u}_p'' \rangle - \frac{1}{\rho_p} \nabla \langle p_p \mathbf{u}_p'' \rangle \tag{5}$$

Finally, the terms left to close are the pressure strain and dissipation terms. These terms are explicitly modelled in the $\overline{v_p^2} - f$ transport equation and are grouped into a source term denoted $k_p f$.

$$k_p f = \underbrace{\phi_{p,yy}}_{\text{pressure strain}} - \underbrace{\varepsilon_{p,yy}}_{\text{dissipation}} + \alpha_p \rho_p 6 \frac{\overline{v_p^2}}{k_p} \varepsilon_p \tag{6}$$

The source term effectively redistributes turbulence energy from the stream-wise Reynolds stress component to the wall-normal component close to walls. This means that particle turbulence energy can only enter the wall-normal component through redistribution. The source term has been shown to overproduce in regions relatively far away from the wall and the correction of Davidson et al. [6] is employed.

$$\overline{v_p^2}_{source} = \min\left\{ k_p f,\ -\frac{1}{T}\left[(C_1 - 6)\overline{v_p^2} - \frac{2k_p}{3}(C_1 - 1)\right] + C_2 \Pi_p \right\} \tag{7}$$

Now setting the wall-normal component of the fluid-phase Reynolds stress tensor $\langle \mathbf{u}_p'' \otimes \mathbf{u}_p'' \rangle_p$ to $\overline{v_p^2}$ a transport equation can be written as:

$$\frac{\partial(\alpha_p \rho_p \overline{v_p^2})}{\partial t} + \nabla \cdot (\alpha_p \rho_p \overline{v_f^2} \mathbf{u}_p) = \nabla \cdot \left(\mu_p + \frac{\mu_{pt}}{\sigma_{pk}}\right) \nabla \overline{v_p^2} + \alpha_p \rho_p \overline{v_p^2}_{source} - \alpha_p \rho_p 6 \frac{\overline{v_p^2}}{k_p} \varepsilon_p + 2\beta(\overline{v_{fp}^2} - \overline{v_p^2}) \tag{8}$$

The reader should note that the third term is a sink term that is used to balance the source term $k_p f$. This is a modification proposed by Lien and Kalitzin [8] and ensures that the source term $k_p f \to 0$ as it approaches the wall.

Eq. 8 contains no sensitivity to the wall distance and thus a modified Helmholtz equation is constructed to form an elliptic relaxation equation. The form of this equation accounts for anisotropy close to walls and is also independent of Reynolds number and y$^+$ value which reads

$$L_p^2 \frac{\partial^2 f}{\partial x^2} - f = \underbrace{\frac{C_1}{T_p}\left(\frac{\overline{v_p^2}}{k_p} - \frac{2}{3}\right)}_{\phi_{p,yy,S}} - \underbrace{C_2 \frac{\Pi_p}{k_p}}_{\phi_{p,yy,R}} - \frac{1}{T_p}\left(6\frac{\overline{v_p^2}}{k_p} - \frac{2}{3}\right) \tag{9}$$

The terms $\phi_{p,yy,S}$ and $\phi_{p,yy,R}$ are the so-called slow and rapid pressure-strain terms [33, 1] with the final term being used to ensure far field behaviour i.e. that the elliptic relaxation function diminishes away from walls. Solving a Poisson equation with a segregated solver can cause numerical issues due to its elliptical nature. This issue can be resolved by following Lien and Kalitzin [8] and introducing a sink and source term in $k_p f$ source term in the $\overline{v_p^2}$ and f transport equation of the form, $6\frac{\overline{v_p^2}}{k_p}$. This enables a Dirichlet boundary condition to be prescribed. The eddy viscosity is calculated from the solution of the $\overline{v_p^2} - f$ model, again the correction proposed by Davidson et al. [6] is used.

$$\nu_{pt} = \min\left\{C_{p\mu} k_p^2/\varepsilon_p,\ C_\mu \overline{v_p^2} T_p\right\} \tag{10}$$

where the turbulent time and length scales are defined in analogy to those in the fluid phase, we can define a characteristic length and time scale based on the particle turbulent flow variables as:

$$\mathrm{T}_p = \max\left(\frac{k_p}{\varepsilon_p}, 6\sqrt{\frac{\nu_f}{\varepsilon_f}}\right) \tag{11}$$

$$\mathrm{L}_p = \max\left(\frac{k_p^{3/2}}{\varepsilon_p}, C_\eta \frac{\nu_f^{3/4}}{\varepsilon_f^{1/4}}\right) \tag{12}$$

Both time and length scales are limited in regions close to the wall. In regions close to the wall k_p need not be zero but due to one-way coupling used in this work the mean slip $\rightarrow 0$ therefore the particles remain correlated. In regions close to the wall the particle characteristic time scale can reduce below the Kolmorgorov scale hence limiting is applied. It is instructive to note that as the particle relaxation time increases closer to the wall and the particles become less responsive to the main flow uncorrelated energy Θ_p is created. Hence, at the correlated macro-scale k_p the production due to the velocity covariance is dominant but as the particle response time increases uncorrelated meso-scale energy Θ_p is produced. As the fluid-particle flow remains correlated the scaling is retained.

2.2. Model setup and solution

The geometry comprises of two flat parallel walls. The computational domain of size $16\pi h$ x $2h$, with x-, y- axes in the stream-wise and wall-normal directions, respectively. Four mesh resolutions are investigated with $y^+ = 0.5$ kept constant throughout with an inflation ratio of 1.1 in the y direction. For smaller y^+ values the computational cost increases dramatically due to the aspect-ratio and simulations become unfeasible.

The wall boundary condition for ε_f can be found in Table 3. For the remaining model variables the following boundary conditions at the wall are prescribed, $\mathbf{u}_f = k_f = \overline{v_f^2} = f = 0$. For the particulate phase a Neumann boundary condition is prescribed for the velocity and turbulence statistics. Both k_p and ε_p are initialised as 1/3rd of their fluid counterpart with $\Theta_p = 1.0 \text{ x } 10^{-8}\text{m}^2\text{s}^{-2}$. At the inlet a Dirichlet boundary condition is prescribed for both phase velocities and a Neumann condition for pressure. At the outlet a Dirichlet boundary condition is prescribed for pressure and a Neumann condition for both phase velocities.

The RA-TFM and the recently derived $\overline{v_p^2} - f$; $\overline{v_f^2} - f$ turbulence models are implemented into the open-source toolbox OpenFOAM [34]. The solver `ratfmFoam` is based on our previous work [26] and is made open-source. To handle the pressure-velocity coupling the Pressure Implicit with Splitting Operators (PISO) algorithm [35, 36] is used. The volume fraction is solved using Multi-dimensional Universal Limiter with Explicit Solution (MULES) [37] which is a flux-corrected transport algorithm which ensures robustness, stability and convergence. Time derivative terms are discretised using the first order accurate implicit Euler, gradients are discretised using the least squares scheme, convective terms are discretised using the second order central scheme (limitedLinearV/limitedLinear01). The former is used for vectors and the latter is used for bounding variables between 0 and 1. Finally, Laplacian schemes are discretised with the second order accurate central differencing scheme.

Table 1: Table of simulated cases

Case	d_p [μm]	ρ_p [kg/m^3]	St
1	20.4	1000	1
2	45.6	1000	5

Table 2: RA-TFM governing equations

Governing equations of the particle-phase:

$$\frac{\partial(\alpha_p\rho_p)}{\partial t} + \nabla\cdot(\alpha_p\rho_p\mathbf{u}_p) = 0 \tag{13}$$

$$\begin{aligned}\frac{\partial(\alpha_p\rho_p\mathbf{u}_p)}{\partial t} + \nabla\cdot(\alpha_p\rho_p\mathbf{u}_p\mathbf{u}_p) = \nabla\cdot 2(\mu_p+\mu_{pt})\overline{\mathbf{S}}_\mathbf{p} + \beta\Big[(\mathbf{u}_f-\mathbf{u}_p) - \frac{\nu_{ft}}{\mathrm{Sc}_{fs}\alpha_p\alpha_f}\nabla\alpha_p\Big] \\ -\nabla p_p - \alpha_p\nabla p_f + \alpha_p\rho_p\Big[1-\alpha_f\Big(1-\frac{\rho_f}{\rho_p}\Big)\Big]\mathbf{g}\end{aligned} \tag{14}$$

Governing and phase-energy equations of the particle-phase:

$$\frac{\partial(\alpha_f\rho_f)}{\partial t} + \nabla\cdot(\alpha_f\rho_f\mathbf{u}_f) = 0 \tag{15}$$

$$\begin{aligned}\frac{\partial(\alpha_f\rho_f\mathbf{u}_f)}{\partial t} + \nabla\cdot(\alpha_f\rho_f\mathbf{u}_f\mathbf{u}_f) = \nabla\cdot 2(\mu_f+\mu_{ft})\overline{\mathbf{S}}_\mathbf{f} + \beta\Big[(\mathbf{u}_p-\mathbf{u}_f) + \frac{\nu_{ft}}{\mathrm{Sc}_{fs}\alpha_p\alpha_f}\nabla\alpha_p\Big] \\ -\alpha_f\nabla p_f + \alpha_p\nabla p_f + \alpha_f\rho_f\Big[1+\alpha_p\Big(\frac{\rho_p}{\rho_f}-1\Big)\Big]\mathbf{g}\end{aligned} \tag{16}$$

$$\begin{aligned}\frac{\partial(\alpha_f\rho_f k_f)}{\partial t} + \nabla\cdot(\alpha_f\rho_f k_f\mathbf{u}_f) = \nabla\cdot\Big(\mu_t + \frac{\mu_{ft}}{\sigma_{fk}}\Big)\nabla k_f + \alpha_f\rho_f\Pi_f - \alpha_f\rho_f\varepsilon_f \\ +2\beta(k_{fp}-k_f)\end{aligned} \tag{17}$$

$$\begin{aligned}\frac{\partial(\alpha_f\rho_f\varepsilon_f)}{\partial t} + \nabla\cdot(\alpha_f\rho_f\varepsilon_f\mathbf{u}_f) = \nabla\cdot\Big(\mu_t + \frac{\mu_{ft}}{\sigma_{fk}}\Big)\nabla\varepsilon_f + \frac{\varepsilon_f}{k_f}\Big[C_{\varepsilon 1}\alpha_f\rho_f\Pi_f - C_{\varepsilon 2}\alpha_f\rho_f\varepsilon_f\Big] \\ +2\beta(\varepsilon_{fp}-\varepsilon_f)\end{aligned} \tag{18}$$

$$\begin{aligned}\frac{\partial(\alpha_f\rho_f\overline{v_f^2})}{\partial t} + \nabla\cdot(\alpha_f\rho_f\overline{v_f^2}\mathbf{u}_f) = \nabla\cdot\Big(\mu_f + \frac{\mu_{ft}}{\sigma_{fk}}\Big)\nabla\overline{v_f^2} + \alpha_f\rho_f\overline{v_f^2}_{source} - \alpha_f\rho_f 6\frac{\overline{v_f^2}}{k_f}\varepsilon_f \\ +2\beta(\overline{v_{fp}^2}-\overline{v_f^2})\end{aligned} \tag{19}$$

$$L^2\frac{\partial^2 f}{\partial x^2} - f = \frac{C_1}{T}\left(\frac{\overline{v_f^2}}{k_f} - \frac{2}{3}\right) - C_2\frac{\Pi_f}{k_f} - \frac{1}{T}\left(6\frac{\overline{v_f^2}}{k_f} - \frac{2}{3}\right) \tag{20}$$

211 ## 3. Results and Discussion

212 ### *3.1. Influence of mesh resolution*

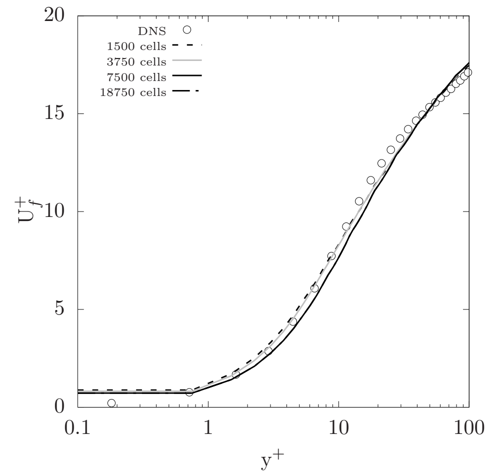

Figure 1: Mean fluid stream-wise velocity convergence

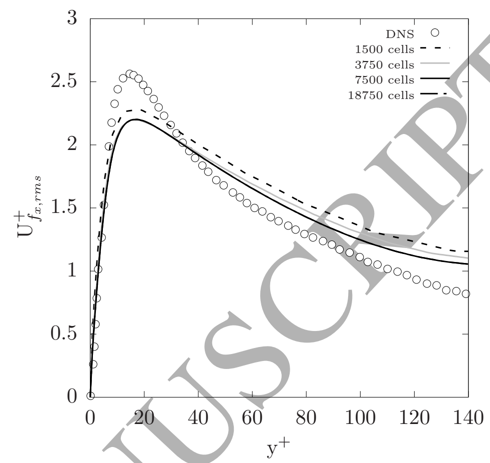

Figure 2: Fluid stream-wise fluctuation velocity convergence

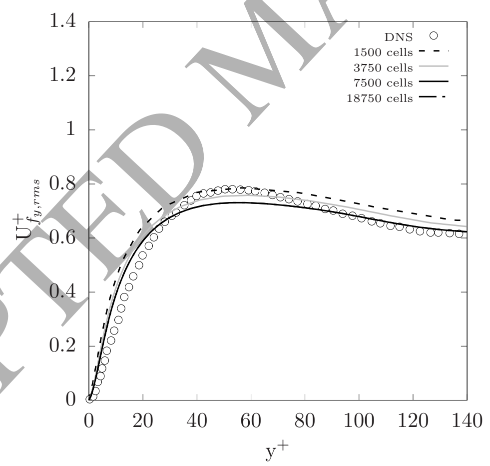

Figure 3: Fluid wall-normal fluctuation velocity convergence

213 To ascertain the influence of the mesh's resolution four different mesh sizes are
214 compared; 1500, 3750, 7500 and 18750 cells pertaining to 25x50, 50x75, 75x100 and

1250x150 in the x- and y- direction, respectively. Simulations are run for 500s of real flow time with all flow statistics being averaged through flow sampling. Flow sampling takes place after 100s and is used to ascertain temporal sensitivity of the solution. For the sake of brevity only the fluid flow statistics are shown here. Figs. [1-3] show that with incremental increases in mesh resolution the results tend towards a converged solution. The final two mesh resolutions reveal no change across all three flow variables. These two mesh resolutions indicate that the solution is mesh independent and no further enhancement of the resolution will change the solution. For the sake of computational cost, and with no loss of accuracy, the former mesh consisting of 7500 cells is used throughout this work.

3.2. Fluid phase

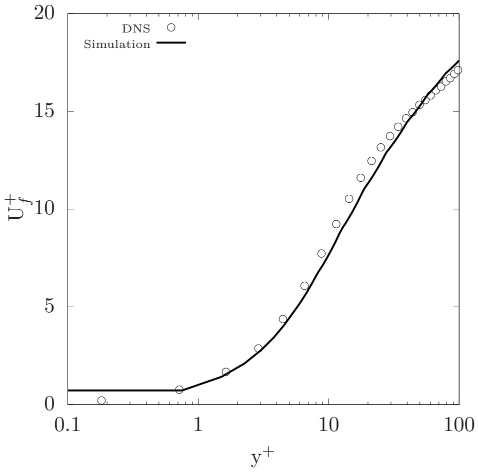

Figure 4: Mean fluid stream-wise velocity

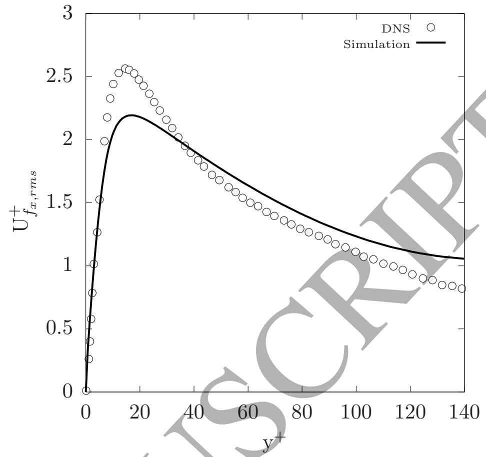

Figure 5: Fluid stream-wise fluctuation velocity

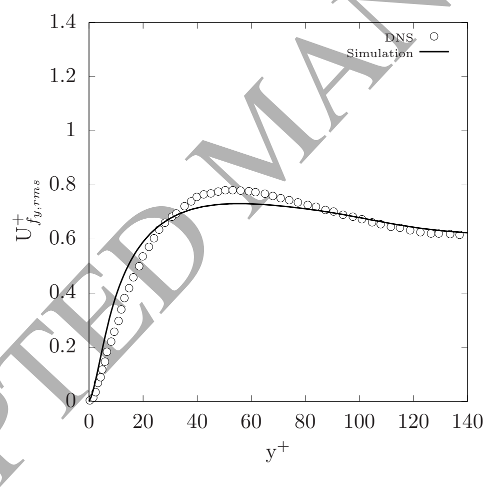

Figure 6: Fluid wall-normal fluctuation velocity

Fig. 4 shows the calculation of the mean fluid-phase velocity. There is a satisfactory prediction of the mean velocity spanning from the viscous wall region to the log-law region. This crucial region for predicting a number of phenomena i.e. heat transfer, particle-wall interaction and compressible flows can be accurately modelled with the $\overline{v_f} - f$ model. From $y^+ < 1$ there exists two mesh cells which explains the perceived lack of gradient in this region, as mentioned in Section 2.2 a computational limit is set for small values of y^+, although the fluid-phase velocity components do correctly tend to 0 as the wall is approached. It is an artifact of the lack of resolution for very small values of y^+ and the logarithmic scaling.

In Fig. 5 the stream-wise fluctuation velocity is shown. Qualitatively the model is in good agreement especially for an E-E simulation. Despite this two main discrepancies can be seen: the under-prediction in the peak of fluid-phase turbulent kinetic energy and the over-prediction of the turbulence decay in the free-stream. Two explanations that perhaps feed into each other can be suggested. The first, if one invokes continuity across the span of the channel it can be imagined that if the production was increased the decay would increase. Thus we can postulate that if the production was increased a larger peak would be displayed and as a result a steeper gradient of decay would be shown.

The peak is governed by the production term, Π_f which is a function of the fluid-phase turbulent viscosity and mean velocity gradients. The latter can be influenced through numerical schemes - in particular the calculation of the gradient [35]. Secondly, due to the relatively small Reynolds number of the flow, $Re_\tau = 150$ the turbulence model can fail to capture the correct turbulent kinetic energy behaviour. This is due to the model being calibrated for high Reynolds number. In Durbin [4] it is shown that for low Reynolds number flow the model over-predicts turbulence in the free stream - a finding that is consistent with damping functions. It should be noted that they also over-predicted the peak which was not the case in this study. It would seem that an element of both are at work, therefore with calibrating of the turbulence constants a more accurate fit could be obtained. It is also worth mentioning that in the data of Marchioli et al. [28] the peak is the region in which the greatest variance was reported. This is true of both phases and highlights the difficulty in predicting a reliable value.

The near-wall behaviour of the wall-normal component has been accurately captured in Fig. 6. A slight underproduction is seen in the peak across the range $40 < y^+ < 80$ which is expected as the value of the stream-wise fluctuating component is also under-predicted. As discussed the wall-normal component receives turbulent kinetic energy through redistribution - therefore the under-prediction is experienced in both components. Overall excellent agreement with the DNS data is found, this provides promising evidence for the application of the $v^2 - f$ model to E-E modelling.

3.3. Particle phase statistics

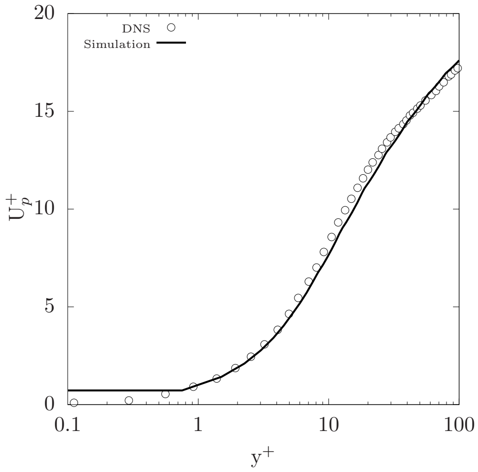

Figure 7: Mean particle stream-wise velocity, St = 1

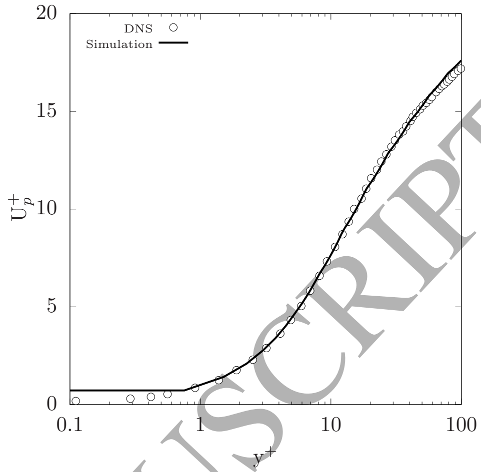

Figure 8: Mean particle stream-wise velocity, St = 5

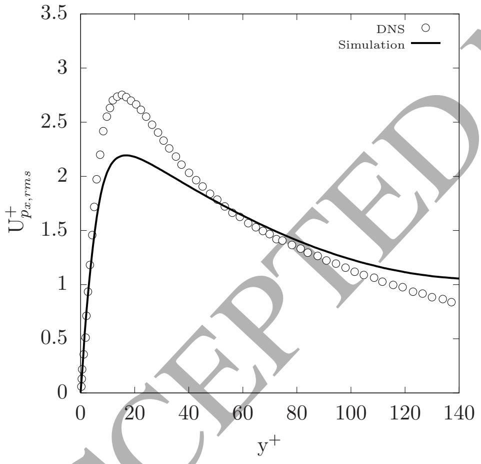

Figure 9: Particle stream-wise fluctuation velocity, St = 1

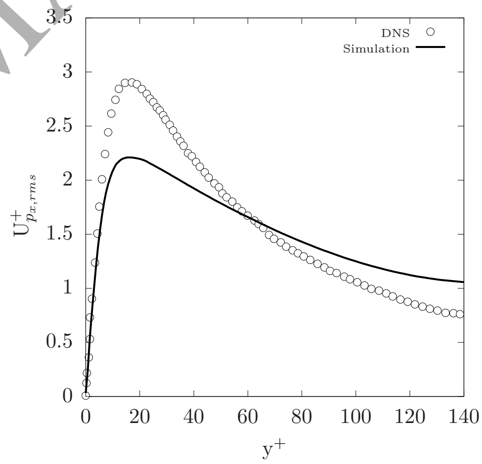

Figure 10: Particle stream-wise fluctuation velocity, St = 5

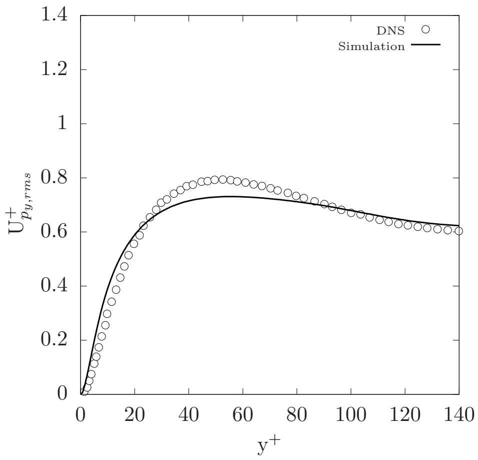

Figure 11: Particle wall-normal fluctuation velocity, St = 1

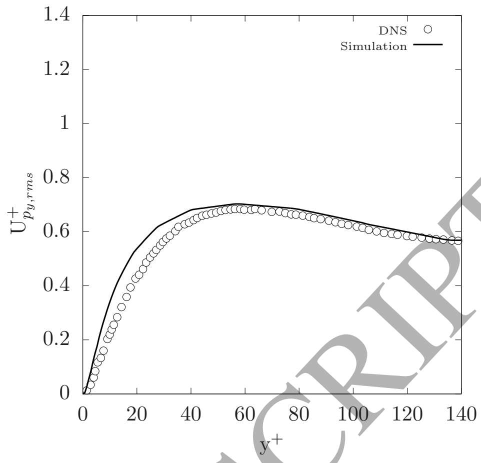

Figure 12: Particle wall-normal fluctuation velocity, St = 5

For the channel flow simulated in the work of Marchioli et al. [28] the fluid-particle co-variance terms dominate the particle-phase energy by providing the major contribution to their production via drag. As the particle phase is one-way coupled with the fluid phase the particles will be dragged along by the fluid and experience no feedback effect on the fluid phase. Even in such a flow it has been shown the need to partition the particle inertia into correlated and uncorrelated motion Fevrier et al. [24]. In the model used throughout this partitioning is denoted by k_p and Θ_p, respectively.

Figs. 7-8 shows the prediction of the particle-phase mean velocity of which shows excellent agreement with the DNS data. The prediction of the mean velocity is well captured across the range of y^+ with the main discrepancy coming from the mesh resolution as discussed previously. Due to the close to non-existent slip velocity, owing to the geometry and governing physics, it is apparent that the von Neumann wall boundary condition results in the correct near-wall behaviour. Owing to the smoothness of the channel no effects due to roughness were incorporated, for further discussion the reader is referred to Vreman [38].

Figs. 9-10 reveal that the model is capable of capturing the Stokes dependent behaviour, which manifests itself in an increase in the peak of turbulent kinetic energy, although the increase is not as large as that seen in the DNS. We recognise here that this increase of particle-phase turbulent kinetic energy is due to the increase in uncorrelated energy, Θ_p. As the particle response time increases the particles become uncorrelated with the main flow. This phenomenon has also been reported by Vance et al. [39], Fevrier et al. [24] who showed that with increasing Stokes number an increasing fraction of the fluctuating energy was found in the random-uncorrelated motion, Θ_p.

We find that the increase in particle response time coupled with the dispersion enhances the "de-correlation" which is why the main increase is seen across $y^+ < 60$. The energy is re-partitioned into the near wall region showing an increase in the peak of the turbulent kinetic energy. As a result over the $y^+ > 60$ there is an increase in the gradient of turbulent kinetic energy decay, a feature that was not captured. It is interesting to note that this re-partitioning of the particle-phase energy is not especially felt in the mean-velocity profile.

In Fig. 10, even though an increase in the peak seen at $y^+ \approx 11.6$ is apparent the behaviour approaching the free-stream is at odds with the DNS data. The lack of turbulent kinetic energy decay is most apparent across $y^+ > 60$. It is clear that the distribution of the turbulence energy changes quite considerably with larger response times and a sharper gradient of decay is shown. This suggests that an adjustment of the the turbulent decay constant could be made a function of the particle Stokes number.

As shown in Marchioli and Soldati [40] preferential concentration is shown for Stokes number 5, a feature that was also seen in the simulation. We find in our simulations that with increasing particle response time particles tended to drift towards the wall becoming preferentially concentrated. A phenomenon that is well-established in the literature Reeks [22]. This behaviour was determined by the drift velocity as expected, which is a function the gradient of volume fraction and Stokes number. Figs. 11-12 show the particle-wall normal fluctuation velocity components. A satisfactory prediction across both simulations can be seen. The main discrepancy is the lack of peak in the former although the trend is captured elsewhere.

4. Conclusions

In this work we have presented a pressure-velocity model for both the particle- and fluid-phase for use in Eulerian-Eulerian simulations. The turbulence model was derived within a Reynolds-Averaged Two-Fluid Model framework and applied to channel flow. Throughout it has been shown that accounting for the kinematic blocking effect leads to promising results. Across both fluid and particle turbulence statistics a good agreement was shown, in particular the wall-normal energy component of each respective phase was well produced. A result that has hitherto alluded E-E simulations. The results were validated against benchmark Direct Numerical Simulation of Marchioli et al. [28] and show strong qualitatively and quantitatively agreement. The RA-TFM shows the correct Stokes dependence behaviour exhibited in the particle-phase turbulence statistics. The current predictions show encouraging results and efforts should be made to extend the approach for more complex flow regimes i.e. two-way coupling.

5. Code repository

The source code of the `ratfmFoam` solver and supplementary material can be downloaded from [41] and is distributed under the terms of the GNU General Public License v3.

6. Acknowledgements

This work has benefited from a PhD Scholarship from the College of Engineering, Mathematics and Physical Sciences at the University of Exeter.

7. Appendix A

We begin with the exact RA Reynolds Stress transport equation for the fluid phase which is found by Reynolds-Averaging the PA velocity tensor transport equation and subtracting the PA fluid-phase mean velocity tensor transport equation. A rigorous derivation can be found in [32] and for the sake of brevity will not be presented here.

$$\begin{aligned}\frac{\partial\langle\alpha_f\rangle\langle\mathbf{u}_f'''\otimes\mathbf{u}_f'''\rangle_f}{\partial t}+\nabla\cdot\langle\alpha_f\rangle\langle\mathbf{u}_f\rangle_f\otimes\langle\mathbf{u}_f'''\otimes\mathbf{u}_f'''\rangle_f &= -\nabla\cdot\langle\alpha_f\rangle\langle\mathbf{u}_f'''\otimes\mathbf{u}_f'''\otimes\mathbf{u}_f'''\rangle_f \\ &-\underbrace{\langle\alpha_f\rangle(\langle\mathbf{u}_f'''\otimes\mathbf{u}_f'''\rangle_f\cdot\nabla\langle\mathbf{u}_f\rangle_f)}_{\text{Production}}+\frac{1}{\rho_f}\nabla\cdot\langle\overline{\boldsymbol{\sigma}}_f\otimes\mathbf{u}_f'''\rangle-\frac{1}{\rho_f}\nabla\langle p_f\mathbf{u}_f'''\rangle \\ +\underbrace{\frac{1}{\rho_f}\langle p_f\nabla\mathbf{u}_f'''\rangle}_{\text{pressure strain, }\phi_{f,yy}} &-\underbrace{\frac{1}{\rho_f}\langle\overline{\boldsymbol{\sigma}}_f\cdot\nabla\mathbf{u}_f'''\rangle}_{\text{dissipation, }\varepsilon_{f,yy}}+\langle\alpha_f\rangle\beta(\underbrace{\langle\mathbf{u}_f'''\otimes\mathbf{u}_p''\rangle_p-\langle\mathbf{u}_f'''\otimes\mathbf{u}_f'''\rangle_p}_{\text{velocity correlations}})\end{aligned} \tag{21}$$

The velocity correlations which arise due to phase coupling are modelled analogously to those terms found in the $k_f-\varepsilon_f$ transport equations. We set the co-variance of the fluctuations $\langle\mathbf{u}_f'''\otimes\mathbf{u}_p''\rangle_p=\overline{v_{fp}^2}=\sqrt{\overline{v_f^2}\,\overline{v_p^2}}$. Following the standard approach used in classic eddy-viscosity turbulence models, the divergence terms appearing in the transport equation are closed by the gradient-diffusion hypothesis [1].

$$\nabla \cdot \left[\frac{\mu_{ft}}{\sigma_{fk}} \nabla \langle \mathbf{u}_f''' \otimes \mathbf{u}_f''' \rangle_f \right] \approx -\nabla \cdot \langle \alpha_f \rangle \langle \mathbf{u}_f''' \otimes \mathbf{u}_f''' \otimes \mathbf{u}_f''' \rangle_f + \frac{1}{\rho_f} \nabla \cdot \langle \overline{\boldsymbol{\sigma}}_f \otimes \mathbf{u}_f''' \rangle - \frac{1}{\rho_f} \nabla \langle p_f \mathbf{u}_f''' \rangle \tag{22}$$

Finally, the terms left to close are the pressure strain and dissipation terms. These terms are explicitly modelled in the $\overline{v_f^2} - f$ transport equation and are grouped into a source term denoted $k_f f$.

$$k_f f = \underbrace{\phi_{f,yy}}_{\text{pressure strain}} - \underbrace{\varepsilon_{f,yy}}_{\text{dissipation}} + \alpha_f \rho_f 6 \frac{\overline{v_f^2}}{k_f} \varepsilon_f \tag{23}$$

The source term effectively redistributes turbulence energy from the stream-wise Reynolds stress component to the wall-normal component close to walls. This is intuitive as previously discussed, when one considers a fully developed turbulent boundary layer as the wall-normal Reynolds stress component's production is zero due to the mean stream-wise flow gradient. This means that turbulence energy can only enter the wall-normal component through redistribution. The source term has been shown to overproduce in regions relatively far away from the wall and the correction of Davidson et al. [6] is employed.

$$\overline{v_f^2}_{source} = \min\left\{ k_f f, -\frac{1}{T}\left[(C_1 - 6)\overline{v_f^2} - \frac{2k_f}{3}(C_1 - 1) \right] + C_2 \Pi_f \right\} \tag{24}$$

Now setting the wall-normal component of the fluid-phase Reynolds stress tensor $\langle \mathbf{u}_f''' \otimes \mathbf{u}_f''' \rangle_f$ to $\overline{v_f^2}$ a transport equation can be written

$$\frac{\partial(\alpha_f \rho_f \overline{v_f^2})}{\partial t} + \nabla \cdot (\alpha_f \rho_f \overline{v_f^2} \mathbf{u}_f) = \nabla \cdot \left(\mu_f + \frac{\mu_{ft}}{\sigma_{fk}} \right) \nabla \overline{v_f^2} + \alpha_f \rho_f \overline{v_f^2}_{source} - \alpha_f \rho_f 6 \frac{\overline{v_f^2}}{k_f} \varepsilon_f + 2\beta(\overline{v_{fp}^2} - \overline{v_f^2}) \tag{25}$$

The reader should note that the third term is a sink term that is used to balance the source term $k_f f$. This is a modification proposed by Lien and Kalitzin [8] and ensures that the source term $k_f f \to 0$ as it approaches the wall.

Eq. 25 contains no sensitivity to the wall distance and thus a modified Helmholtz equation is constructed to form an elliptic relaxation equation. The form of this equation accounts for anisotropy close to walls and is also independent of Reynolds number and y^+ value which reads

$$L^2 \frac{\partial^2 f}{\partial x^2} - f = \underbrace{\frac{C_1}{T}\left(\frac{\overline{v_f^2}}{k_f} - \frac{2}{3}\right)}_{\phi_{f,yy,S}} - \underbrace{C_2 \frac{\Pi_f}{k_f}}_{\phi_{f,yy,R}} - \frac{1}{T}\left(6\frac{\overline{v_f^2}}{k_f} - \frac{2}{3}\right) \tag{26}$$

The terms $\phi_{f,yy,S}$ and $\phi_{f,yy,R}$ are the so-called slow and rapid pressure-strain terms [1, 33] with the final term being used to ensure far field behaviour i.e. that the elliptic relaxation function diminishes away from walls.

One drawback of employing a methodology that requires the solution of Poisson's equation is its elliptic nature. When solving the equation with a segregated solver as in this work a numerical problem arises as information from upstream is not available. To circumvent these issues Lien and Kalitzin [8] introduced the $6\frac{\overline{v_f^2}}{k_f}$ as a sink and source in $k_f f$ source term in the $\overline{v_f^2}$ transport equation. It is also introduced in the transport equation of f. This ensures that f correctly tends to 0 at a wall allowing a Dirichlet boundary condition to be prescribed. The eddy viscosity is calculated from the solution of the $\overline{v_f^2} - f$ model, again the correction proposed by Davidson et al. [6] is used.

$$\nu_{ft} = \min\left\{C_{f\mu} k_f^2/\varepsilon_f,\ C_\mu \overline{v_f^2} T\right\} \tag{27}$$

where the turbulent time and length scales are defined as

$$\mathrm{T} = \max\left(\frac{k_f}{\varepsilon_f}, 6\sqrt{\frac{\nu_f}{\varepsilon_f}}\right) \tag{28}$$

$$\mathrm{L} = \max\left(\frac{k_f^{3/2}}{\varepsilon_f}, C_\eta \frac{\nu_f^{3/4}}{\varepsilon_f^{1/4}}\right) \tag{29}$$

Both time and length scales are limited in regions close to the wall. This is achieved by introducing a dependency on Kolmogorov scales which are only active in regions very close to the wall i.e. $y^+ < 5$. This ensures that a singularity is not introduced into the solution matrix and that the scales collapse at the wall.

388 **Nomenclature**

C_D	drag coefficient, $[-]$
Re_p	particle Reynolds number, $[-]$
d_p	particle diameter, [m]
$\mathbf{u}_i$	velocity, $[ms^{-1}]$
p_i	pressure, [Pa]
g_0	radial distribution coefficient, $[-]$
t	time, [s]
k_i	turbulent kinetic energy, $[m^2s^{-2}]$

389 *Greek letters*

α_i	volume fraction, $[-]$
$\alpha_{p,max}$	maximum particle volume fraction, $[-]$
β	momentum exchange coefficient, $[kgm^{-3}s^{-1}]$
ε_i	turbulent kinetic energy dissipation, $[m^2s^{-3}]$
Θ_p	granular temperature, $[m^2s^{-2}]$
κ_p	particle fluctuation energy, $[m^2s^{-2}]$
$\kappa_{\Theta s}$	diffusion coefficient for granular energy, $[kgm^{-1}s^{-1}]$
μ_i	shear viscosity, $[kgm^{-1}s^{-1}]$
$\mu_{i,t}$	turbulent shear viscosity, $[kgm^{-1}s^{-1}]$
ν_i	kinematic viscosity, $[m^2s^{-1}]$
$\nu_{i,t}$	turbulent kinematic viscosity, $[m^2s^{-1}]$
ρ_i	density, $[kgm^{-3}]$
$\overline{\boldsymbol{\sigma}}_f$	fluid phase stress tensor,$[kgm^{-1}s^{-2}]$
$\overline{\boldsymbol{\sigma}}_p$	particle phase stress tensor, $[kgm^{-1}s^{-2}]$
τ_d	particle relaxation time, [s]

390 *Subscripts*

f	fluid
i	general index
p	particle
x	x direction
y	y direction
z	z direction
i, yy	wall normal component w.r.t each phase

391 *Superscripts*

$''$	PA particle velocity fluctuation
$'''$	PA fluid velocity fluctuation

392 *Special notation*

$\langle \cdot \rangle$	Reynolds averaging operator
$\langle \cdot \rangle_i$	phase averaging operator associated with phase i

Table 3: Model characteristics & turbulence variables.

$$\beta = \frac{\rho_p \alpha_p}{\tau_d} = \frac{3}{4}\frac{\alpha_p \alpha_f \rho_f \mathbf{u}_r}{d_p} C_d$$

$$C_d = \begin{cases} \frac{24}{Re_p}\left[1 + 0.15 Re_p^{0.287}\right] & \text{if } Re_p < 1000 \\ 0.44 & \text{if } Re_p \geq \ 1000 \end{cases}$$

$$u_{p_{rms}} = \kappa_p = k_p + 3/2\Theta_p$$

$$St = \tau_d/\tau_f$$

$$\tau_f = k_f/\varepsilon_f$$

$$e = 1$$

$$\Pi_p = 2\nu_{pt}\overline{\mathbf{S}}_\mathbf{p} : \overline{\mathbf{S}}_\mathbf{p} + \frac{2}{3}k_p \nabla \cdot \mathbf{u}_p$$

$$\Pi_f = 2\nu_{ft}\overline{\mathbf{S}}_\mathbf{f} : \overline{\mathbf{S}}_\mathbf{f} + \frac{2}{3}k_f \nabla \cdot \mathbf{u}_f$$

$$\varepsilon_f \to 2\nu_f \frac{k_f}{\mathrm{y}^2}$$

$$\mathrm{T} = \max\left(\frac{k_f}{\varepsilon_f}, 6\sqrt{\frac{\nu_f}{\varepsilon_f}}\right)$$

$$\mathrm{L} = \max\left(\frac{k_f^{3/2}}{\varepsilon_f}, C_\eta \frac{\nu_f^{3/4}}{\varepsilon_f^{1/4}}\right)$$

$C_{\varepsilon 1}$	$C_{\varepsilon 2}$	C_μ	C_1	C_2	C_L	C_η	β_ϵ	$C_{f\mu}$	$C_{p\mu}$	σ_k	σ_ϵ
1.6	1.9	0.22	1.4	0.3	0.23	70	1	0.09	0.09	1	1

Table 4: Definition of variables.

$$\kappa_p = k_p + 1.5\Theta_p$$

$$\mu_f = \rho_f \nu_f$$

$$\mu_{ft} = \alpha_f \rho_f \nu_{ft} = \alpha_f \rho_f C_\mu \overline{v_f^2} T$$

$$\mu_p = \alpha_p \rho_p \nu_p = \frac{2\mu_{p_{dil}}}{(1+e)g_0}\Big[1 + \frac{4}{5}(1+e)g_0\alpha_p\Big]^2 + \frac{4}{5}\alpha_p^2\rho_p d_p g_0(1+e)\Big(\frac{\Theta_p}{\pi}\Big)^{1/2}$$

$$\mu_{p_{dil}} = \frac{5\sqrt{\pi}}{96}\rho_p d_p \Theta_p^{1/2}$$

$$\mu_{pt} = \alpha_p \rho_p \nu_{pt} = \alpha_p \rho_p C_\mu \overline{v_f^2} T$$

$$\mathrm{p}_p = \rho_p \alpha_p \Theta_p + 2(1+e)\rho_p \alpha_p^2 g_0 \Theta_p$$

$$\gamma = \frac{12(1-e^2)g_o}{\sqrt{\pi} d_p}\alpha_p^2 \rho_p \Theta_p^{3/2}$$

$$\kappa_\Theta = \frac{2}{(1+e)g_0}\Big[1 + \frac{6}{5}(1+e)g_0\alpha_p\Big]^2 \kappa_{\Theta,dil} + 2\alpha_p^2\rho_p d_p g_0(1+e)\Big(\frac{\Theta_p}{\pi}\Big)^{\frac{1}{2}}$$

$$\kappa_{\Theta,dil} = \frac{75}{384}\sqrt{\pi}\rho_p d_p \Theta_p^{1/2}$$

$$g_0 = \Big[1 - \Big(\frac{\alpha_p}{\alpha_{p,max}}\Big)^{\frac{1}{3}}\Big]^{-1}$$

$$\overline{\mathbf{S}}_\mathbf{p} = \frac{1}{2}[\nabla \mathbf{u}_p + (\nabla \mathbf{u}_p)^T] - \frac{1}{3}\nabla \cdot \mathbf{u}_p \mathbf{I}$$

$$\overline{\mathbf{S}}_\mathbf{f} = \frac{1}{2}[\nabla \mathbf{u}_f + (\nabla \mathbf{u}_f)^T] - \frac{1}{3}\nabla \cdot \mathbf{u}_f \mathbf{I}$$

$$k_{fp} = \beta_k \sqrt{k_f k_p}$$

$$\varepsilon_{fp} = \beta_\varepsilon \sqrt{\varepsilon_f \varepsilon_p}$$

$$\overline{v_{fp}^2} = \beta_v \sqrt{\overline{v_f^2}\,\overline{v_p^2}}$$

Table 5: Definition of phase-averaged variables.

$$\alpha_p = \langle \alpha_p \rangle$$

$$\alpha_f = \langle \alpha_f \rangle$$

$$\mathbf{u}_p = \langle \mathbf{u} \rangle_p$$

$$\mathbf{u}_f = \langle \mathbf{u} \rangle_f$$

$$\Theta_p = \langle \Theta \rangle_p$$

$$k_p = \frac{1}{2} \langle \mathbf{u}_p'' \cdot \mathbf{u}_p'' \rangle_p$$

$$k_f = \frac{1}{2} \langle \mathbf{u}_f''' \cdot \mathbf{u}_f''' \rangle_f$$

$$\varepsilon_p = \frac{1}{\rho_p \alpha_p} \langle \bar{\boldsymbol{\sigma}}_p : \nabla \mathbf{u}_p'' \rangle$$

$$\varepsilon_f = \frac{1}{\rho_f \alpha_f} \langle \bar{\boldsymbol{\sigma}}_f : \nabla \mathbf{u}_f''' \rangle$$

$$\overline{\boldsymbol{\sigma}}_p = \mu_p [\nabla \mathbf{u}_p + (\nabla \mathbf{u}_p)^T] - \frac{1}{3} \mu_p \nabla \cdot \mathbf{u}_p \mathbf{I}$$

$$\overline{\boldsymbol{\sigma}}_f = \mu_f [\nabla \mathbf{u}_f + (\nabla \mathbf{u}_f)^T] - \frac{1}{3} \mu_f \nabla \cdot \mathbf{u}_f \mathbf{I}$$

$$\mathbf{u}_p'' = \mathbf{u}_p - \langle \mathbf{u}_p \rangle_p$$

$$\mathbf{q}_\Theta = \langle \mathbf{q}_\Theta \rangle_p = \frac{\kappa_\Theta}{\alpha_p \rho_p} \nabla \Theta_p$$

$$\mathbf{u}_f''' = \mathbf{u}_f - \langle \mathbf{u}_f \rangle_f$$

$$\langle \mathbf{u}_p \rangle_p = \langle \alpha_p \mathbf{u}_p \rangle / \langle \alpha_p \rangle$$

$$\langle \mathbf{u}_f \rangle_f = \langle \alpha_f \mathbf{u}_f \rangle / \langle \alpha_f \rangle$$

$$\mathbf{u}_p'' \mathbf{u}_p'' = \langle \mathbf{u}_p'' \mathbf{u}_p'' \rangle_p$$

8. Bibliography

References

[1] S. B. Pope, *Turbulent flows.* Cambridge: Cambridge Univ. Press, 2011.

[2] J. C. R. Hunt and J. M. R. Graham, "Free-stream turbulence near plane boundaries," *Journal of Fluid Mechanics*, vol. 84, no. 2, pp. 209–235, 1978.

[3] N. H. Thomas and P. E. Hancock, "Grid turbulence near a moving wall," *Journal of Fluid Mechanics*, vol. 82, no. 3, pp. 481–496, 1977.

[4] P. A. Durbin, "Near-wall turbulence closure modeling without "damping functions"," *Theoretical and Computational Fluid Dynamics*, vol. 3, no. 1, pp. 1–13, Sep 1991. [Online]. Available: https://doi.org/10.1007/BF00271513

[5] M. Behnia, S. Parneix, and P. Durbin, "Prediction of heat transfer in an axisymmetric turbulent jet impinging on a flat plate," *International Journal of Heat and Mass Transfer*, vol. 41, no. 12, pp. 1845 – 1855, 1998. [Online]. Available: http://www.sciencedirect.com/science/article/pii/S0017931097002548

[6] L. Davidson, P. V. Nielsen, and A. Sveningsson, "Modifications of the v2-f model for computing the flow in a 3d wall jet," in *Turbulence, heat and mass transfer*, K. Hanjalić, Y. Nagano, and M. Tummers, Eds., 2003, pp. 577–584.

[7] P. A. Durbin and B. A. P. Reif, *Statistical theory and modeling of turbulence flow.* John Wiley & Sons, Ltd, 2010, pp. 109–154. [Online]. Available: http://dx.doi.org/10.1002/9780470972076.ch6

[8] F.-S. Lien and G. Kalitzin, "Computations of transonic flow with the v2-f turbulence model," *International Journal of Heat and Fluid Flow*, vol. 22, no. 1, pp. 53–61, 2001. [Online]. Available: http://www.sciencedirect.com/science/article/pii/S0142727X00000734

[9] A. Sveningsson, "Analysis of the Performance of Different v2f Turbulence Models in a Stator Vane Passage Flow," Ph.D. dissertation, Chalmers University of Technology, 2003.

[10] M. A. Rizk and S. E. Elghobashi, "A two-equation turbulence model for dispersed dilute confined two-phase flows," *International Journal of Multiphase Flow*, vol. 15, no. 1, pp. 119–133, 1989.

[11] B. Vreman, B. J. Geurts, N. G. Deen, J. A. M. Kuipers, and J. G. M. Kuerten, "Two- and four-way coupled euler–lagrangian large-eddy simulation of turbulent particle-laden channel flow," *Flow, Turbulence and Combustion*, vol. 82, no. 1, pp. 47–71, Jan 2009. [Online]. Available: https://doi.org/10.1007/s10494-008-9173-z

[12] S. Benyahia, M. Syamlal, and T. J. O'Brien, "Evaluation of boundary conditions used to model dilute, turbulent gas/solids flows in a pipe," *Powder Technology*, vol. 156, no. 2, pp. 62 – 72, 2005, particle Technology Forum Special Issue. [Online]. Available: http://www.sciencedirect.com/science/article/pii/S0032591005001245

[13] A. Benavides and B. van Wachem, "Numerical simulation and validation of dilute turbulent gas-particle flow with inelastic collisions and turbulence modulation," *Powder Technology*, vol. 182, pp. 294–306, 2008.

[14] S. Dasgupta, R. Jackson, and S. Sundaresan, "Turbulent gas-particle flow in vertical risers," *AIChE Journal*, vol. 40, no. 2, pp. 215–228, 1994. [Online]. Available: http://dx.doi.org/10.1002/aic.690400204

[15] Y. Reinhardt and L. Kleiser, "Validation of Particle-Laden Turbulent Flow Simulations Including Turbulence Modulation," *Journal of Fluids Engineering*, vol. 137, no. 7, p. 71303, 2015.

[16] M. T. Shah, R. P. Utikar, V. K. Pareek, M. O. Tade, and G. M. Evans, "Effect of closure models on eulerian-eulerian gas-solid flow predictions in riser," *Powder Technology*, vol. 269, pp. 247 – 258, 2015. [Online]. Available: http://www.sciencedirect.com/science/article/pii/S0032591014007785

[17] T. Strömgren, G. Brethouwer, G. Amberg, and A. V. Johansson, "Modelling of turbulent gas-particle flows with focus on two-way coupling effects on turbophoresis," *Powder Technology*, vol. 224, pp. 36–45, 2012. [Online]. Available: http://dx.doi.org/10.1016/j.powtec.2012.02.017

[18] E. J. Bolio, J. A. Yasuna, and J. L. Sinclair, "Dilute turbulent gas-solid flow in risers with particle-particle interactions," *AIChE Journal*, vol. 41, no. 6, pp. 1375–1388, 1995.

[19] S. Dasgupta, R. Jackson, and S. Sundaresan, "Gas-particle flow in vertical pipes with high mass loading of particles," *Powder Technology*, vol. 96, no. 1,

pp. 6 – 23, 1998. [Online]. Available: http://www.sciencedirect.com/science/article/pii/S0032591097033482

[20] Y. Zheng, X. Wan, Z. Qian, F. Wei, and Y. Jin, "Numerical simulation of the gas-particle turbulent flow in riser reactor based on k-ϵ-kp-ϵp-θ two-fluid model," *Chemical Engineering Science*, vol. 56, no. 24, pp. 6813–6822, 2001.

[21] V. C. Patel, W. Rodi, and G. Scheuerer, "Turbulence models for near-wall and low Reynolds number flows - A review," *AIAA Journal*, vol. 23, no. 9, pp. 1308–1319, 1985. [Online]. Available: http://arc.aiaa.org/doi/abs/10.2514/3.9086

[22] M. Reeks, "The transport of discrete particles in inhomogeneous turbulence," *Journal of Aerosol Science*, vol. 14, no. 6, pp. 729 – 739, 1983. [Online]. Available: http://www.sciencedirect.com/science/article/pii/0021850283900551

[23] Y. Yamamoto, M. Potthoff, T. Tanaka, T. Kajishima, and Y. Tsuji, "Large-eddy simulation of turbulent gas-particle flow in a vertical channel: effect of considering inter-particle collisions," *Journal of Fluid Mechanics*, vol. 442, pp. 303–334, 2001.

[24] P. Fevrier, O. Simonin, and K. D. Squires, "Partitioning of particle velocities in gas solid turbulent flows into a continuous field and a spatially uncorrelated random distribution: theoretical formalism and numerical study," *Journal of Fluid Mechanics*, vol. 533, pp. 1–46, 2005.

[25] R. O. Fox, "On multiphase turbulence models for collisional fluid-particle flows," *Journal of Fluid Mechanics*, vol. 742, pp. 368–424, 2014.

[26] M. Riella, R. Kahraman, and G. Tabor, "Reynolds-averaged two-fluid model prediction of moderately dilute fluid-particle flow over a backward-facing step," *International Journal of Multiphase Flow*, vol. 106, pp. 95 – 108, 2018. [Online]. Available: https://www.sciencedirect.com/science/article/pii/S0301932217309850

[27] E. Peirano and B. Leckner, "Fundamentals of turbulent gas-solid flows applied to circulating fluidized bed combustion," *Doktorsavhandlingar vid Chalmers Tekniska Hogskola*, vol. 24, no. 1381, pp. 259–296, 1998.

[28] C. Marchioli, A. Soldati, J. Kuerten, B. Arcen, A. Tanière, G. Goldensoph, K. Squires, M. Cargnelutti, and L. Portela, "Statistics of particle dispersion in direct numerical simulations of wall-bounded turbulence: Results of

an international collaborative benchmark test," *International Journal of Multiphase Flow*, vol. 34, no. 9, pp. 879 – 893, 2008. [Online]. Available: http://www.sciencedirect.com/science/article/pii/S0301932208000414

[29] M. Riella, "Turbulence modelling of fluid-particle interaction," Ph.D. dissertation, University of Exeter, 2019.

[30] M. Syamlal and T. J. O'Brien, "Computer simulation of bubbles in a fluidized bed," *AIChE Symposium Series*, vol. 85, no. 270, pp. 22–31, 1989.

[31] B. G. M. Van Wachem, J. C. Schouten, C. M. Van den Bleek, R. Krishna, and J. L. Sinclair, "Comparative analysis of CFD models of dense gas-solid systems," *AIChE Journal*, no. 5, 2001.

[32] J. Capecelatro, O. Desjardins, and R. O. Fox, "On fluid-particle dynamics in fully developed cluster-induced turbulence," *Journal of Fluid Mechanics*, vol. 780, pp. 578–635, 2015.

[33] B. E. Launder, G. J. Reece, and W. Rodi, "Progress in the development of a reynolds-stress turbulence closure," *Journal of Fluid Mechanics*, vol. 68, no. 3, pp. 537–566, 1975.

[34] H. G. Weller, G. Tabor, H. Jasak, and C. Fureby, "A tensorial approach to computational continuum mechanics using object-oriented techniques," *Computers in Physics*, vol. 12, no. 6, pp. 620–631, 1998.

[35] J. H. Ferziger and M. Peric, *Computational Methods for Fluid Dynamics*. Springer, 2002.

[36] R. I. Issa, "Solution of the implicitly discretised fluid flow equations by operator-splitting," *Journal of Computational Physics*, vol. 62, no. 1, pp. 40–65, 1986.

[37] S. T. Zalesak, "Fully multidimensional flux-corrected transport algorithms for fluids," *Journal of Computational Physics*, vol. 31, no. 3, pp. 335–362, 1979.

[38] A. W. Vreman, "Turbulence attenuation in particle-laden flow in smooth and rough channels," *Journal of Fluid Mechanics*, vol. 773, pp. 103–136, 2015.

[39] M. W. Vance, K. D. Squires, and O. Simonin, "Properties of the particle velocity field in gas-solid turbulent channel flow," *Physics of Fluids*, vol. 18, no. 6, p. 063302, 2006.

[40] C. Marchioli and A. Soldati, "Mechanisms for particle transfer and segregation in a turbulent boundary layer," *Journal of Fluid Mechanics*, vol. 468, pp. 283–315, 2002.

[41] M. Riella, "ratfmfoam: A reynolds-averaged two-fluid solver for openfoam-2.2.2." dec 2018, https://github.com/mjriella/ratfmFoam. [Online]. Available: https://doi.org/10.5281/zenodo.2301515